Quantum frequency conversion with ultra-broadband tuning in a Raman memory

Bustard, Philip J.; England, Duncan G.; Heshami, Khabat; Kupchak, Connor; Sussman, Benjamin J.

National Research Council Canada   Conseil national de recherches Canada

Canada

Quantum frequency conversion with ultra-broadband tuning in a Raman memory

Philip J. Bustard,[1] Duncan G. England,[1] Khabat Heshami,[1] Connor Kupchak,[1,2] and Benjamin J. Sussman[1,2,*]

[1]*National Research Council of Canada, 100 Sussex Drive, Ottawa, Ontario, Canada K1A 0R6*
[2]*Department of Physics, University of Ottawa, Ottawa, Ontario, Canada K1N 6N5*

Quantum frequency conversion is a powerful tool for the construction of hybrid quantum photonic technologies. Raman quantum memories are a promising method of conversion due to their broad bandwidths. Here we demonstrate frequency conversion of THz-bandwidth, fs-duration photons at the single-photon level using a Raman quantum memory based on the rotational levels of hydrogen molecules. We shift photons from 765 nm to wavelengths spanning from 673 to 590 nm—an absolute shift of up to 116 THz. We measure total conversion efficiencies of up to 10% and a maximum signal-to-noise ratio of 4.0(1):1, giving an expected conditional fidelity of 0.75, which exceeds the classical threshold of 2/3. Thermal noise could be eliminated by cooling with liquid nitrogen, giving noiseless conversion with wide tunability in the visible and infrared.

The inception of nonlinear optics was heralded with the first demonstration of its most dramatic manifestation: optical frequency conversion [1]. As the research area has matured, methods of frequency conversion have remained at the forefront of technological development; a vast array of phenomena have been exploited and investigated [2], not least stimulated Raman scattering [3]. The continued rapid development of quantum photonic technologies, including photon sources [4], quantum memories [5,6], and detectors [4], has lent further impetus to frequency conversion research because the optimal operating parameters for these devices are often vastly different in wavelength. This wavelength specificity may limit our ability to construct the efficient hybrid technologies necessary for quantum communication [7,8] and optical quantum computing [9], for example.

Several nonlinear phenomena have been used to demonstrate frequency conversion at the quantum level, including sum-frequency generation [10–14], difference-frequency generation [15–18], Bragg-type four-wave mixing (FWM) [19–22], photon-phonon translation in a cavity-optomechanical system [23], and FWM in an ultracold atomic memory [24]. A variety of challenges remain despite these efforts, including low efficiencies, restricted tunability and bandwidth due to use of resonance effects or phase matching constraints, and corruption of the optical signal due to deleterious noise effects. Recently, an ultrafast quantum memory, based on stimulated Raman scattering in bulk diamond, was used to modify the frequency and bandwidth of heralded single photons [25]. Heralded photons from a parametric down-conversion source were shifted by up to ±12 nm from 723 nm. However, thermal noise [Fig. 1(a)] and FWM noise [Fig. 1(b)] degraded the fidelity of the conversion process; the former can be reduced by cooling, but FWM noise in diamond can only be partially suppressed by increasing the diamond length until dispersion limits the phase matching of the FWM [26]. This dispersion also restricts the possible tuning range to $\approx\pm12$ nm, or $\approx\pm5.6$ THz [25]. The trade-off between tuning range and noise is a fundamental limitation of the diamond memory which restricts its potential applications.

We recently demonstrated that FWM noise can be eliminated using the polarization selection rules of a Raman quantum memory based on the rotational levels of hydrogen molecules [27]. Hydrogen has a broad transparency window and low dispersion, stretching from the infrared to the ultraviolet; as a result, it is well-suited for frequency conversion of broadband femtosecond-picosecond duration photons. Indeed, it has previously been used as a nonlinear medium for the generation of ultrabroadband pulse sequences [28,29]. In this article, we demonstrate broadband frequency conversion at the single-photon level using a Raman quantum memory on the rotational levels of hydrogen molecules. We shift THz-bandwidth, fs-duration photons at 765 nm continuously over wavelengths spanning from 673 to 590 nm—a range of 62 THz, and an absolute shift of up to 116 THz. The low dispersion in hydrogen allows for a $\times20$ increase in the available tuning bandwidth compared to diamond, while the elimination of FWM means that this tuning does not create additional noise photons. The large tuning bandwidth demonstrated herein spans the operational wavelengths of a range of nascent quantum devices, including, for example, SiV centers in diamond (730 nm) [30], NV centers (637 nm) [31], Rb at 795 nm [24], and several rare-earth ion-doped crystals [32]. In the future, tuning the wavelength of the input signal will further expand the possible range of operation.

The molecular memory uses off-resonant Raman scattering [33,34] to map photons to, and from, a collective rotational excitation in an ensemble of hydrogen molecules. The memory operation is outlined in Fig. 1(c), which shows the relevant energy levels of the system. The ground level is the $J = 1$ rotational level; the storage level is the $J = 3$ rotational level. In the *write* step, a strong write pulse with frequency ω_w and a weak *signal* pulse with frequency ω_i are applied in two-photon resonance with the splitting Ω between the ground and storage levels, such that $\omega_w = \omega_i - \Omega$. This stimulates a Stokes Raman transition as the signal photon is annihilated and mapped to population in the storage level, with excess energy carried off by the write pulse. To complete the frequency conversion, a read pulse with frequency $\omega_r \neq \omega_w$ is applied. This induces an anti-Stokes Raman transition, and the signal photon is re-emitted from the ensemble with frequency $\omega_o = \omega_r + \Omega$ as population is mapped back to the ground level.
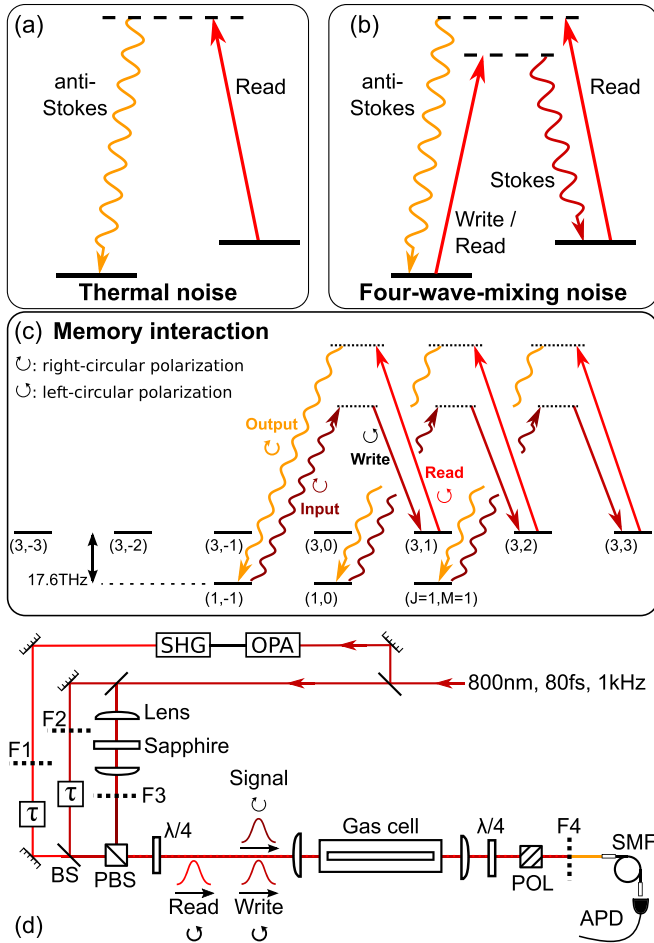
*ben.sussman@nrc.ca

053816-1

FIG. 1. (a) A read pulse scatters from thermal population to create an anti-Stokes noise photon at the signal wavelength. (b) Raman FWM noise: a write (or read) photon scatters to create a Stokes photon and a phonon; a read pulse scattering from the phonon creates an anti-Stokes noise photon. (c) The memory interaction with FWM noise eliminated by selection rules, and (d) the experiment layout.

Hydrogen is a homonuclear, diatomic molecule; its ro-vibrational levels are labeled by the vibrational quantum number v and rotational quantum number J. Each J level is $(2J + 1)$ degenerate with projections $M = -J, -J + 1, ..., J - 1, J$ along the quantization axis. At room temperature $T = 295$ K, hydrogen's population is distributed between the rotational levels, $J = 0, 1, 2, 3$ of the $v = 0$ vibrational level [35]. Due to the rotational level spacings and the equilibrium 3 : 1 ratio of *ortho-*:*para*-hydrogen dictated by nuclear spin statistics, 66% of the population resides in the threefold degenerate $J = 1$ level and 8.8% of the population resides in the sevenfold degenerate $J = 3$ level; this population gives rise to thermal noise. We therefore use the $(J = 1, M)$ states as the ground level and the corresponding $(J = 3, M + 2)$ states as the storage level; the frequency separation of these levels is $\Omega/(2\pi) = 17.6$ THz [35,36].

The selection rules for rotational Raman transitions are $\Delta J = \pm 2$, and $\Delta M = 0, \pm 2$. With the propagation direction taken along the quantization axis, the $\Delta M = \pm 2$ transitions are driven by photons with opposite circular polarization [37]. Thus, a right-circular polarized input signal photon and a left-

circular polarized write pulse drive transitions from $(J = 1, M)$ to $(J = 3, M + 2)$. Crucially, in this scenario, the left-circular polarized write and read pulses cannot drive population into the $(J = 3, M + 2)$ states by Stokes Raman scattering; as a result, noise photons are not created by FWM when the left-circular read pulse is applied [27].

Figure 1(d) shows a diagram of the experiment setup. The master laser for the experiment is a home-built Ti:sapphire amplifier operating at 1 kHz; it outputs 80-fs full-width at half-maximum (FWHM) duration pulses, with FWHM bandwidth $\Delta\lambda = 12$ nm centered at 800 nm. The laser output is partitioned into three beams: write, read, and signal. Write pulses are spectrally filtered (F2) to give an input bandwidth of $\Delta\lambda_w = 4.1$ nm. The read beam pumps an optical parametric amplifier (OPA) to generate down-converted pulses at 1150–1400 nm; type-I second harmonic generation (SHG) in a beta-barium borate (BBO) crystal generates read pulses which can be tuned from $\lambda_r = 590$–700 nm. Spectral filters (F1) are used to limit the read pulses' bandwidth to 5.4–6.1 nm. Signal pulses are spectrally broadened by continuum generation in a sapphire plate [38] to generate photons at 765 nm; additional wavelengths are removed by spectral filters (F3) to give an input signal bandwidth of $\Delta\lambda_i = 9.9$ nm, and neutral density filters attenuate the signal beam to the single-photon level. The relative delays of the three pulses are controlled using motorized delay lines (τ) in the write and read arms. Horizontally polarized write and read pulses are combined at a dichroic beam-splitter (BS) before collinear combination with the vertically polarized input signal pulse at a polarizing beam splitter (PBS). An achromatic quarter-wave plate ($\lambda/4$) converts the write and read pulses to left-circular polarization, and the signal pulse to right-circular polarization. All three pulses are focused collinearly using a 40-cm singlet lens into a 35-cm-long hollow-core capillary with inner diameter 100 μm. The capillary is mounted in a 50-cm-long gas cell, filled with hydrogen gas pressures up to 19.6 bar. The theoretical transmission for the EH_{11} capillary mode is $T_w = 0.47$ for the write pulses, $T_{sig} = 0.50$ for the input signal pulse, and ranges from 0.58 at 673 nm, up to 0.66 at 590 nm [39]. At the output of the gas cell, the three beams are collimated using a 15-cm singlet lens and converted back to linear polarization using a quarter-wave plate. The signal pulse is separated from the write and read beams by polarization (POL) and spectral filtering (F4) [27]. The signal beam is then coupled to an avalanche photodiode (APD) using a single-mode fiber (SMF).

Figure 2 shows the normalized spectra of the input write pulse at $\lambda_w = 800$ nm, the input signal pulse at $\lambda_i = 765$ nm, and the output signal pulse at four central frequencies: $\lambda_o = 590$ nm, 610 nm, 640 nm, and 673 nm. In what follows, we characterize the frequency conversion capabilities of the memory at these example wavelengths; the read pulse is fixed at a delay of $\approx$4 ps relative to the input signal pulse.

In order to confirm operation at the quantum level, we attenuated the input 765-nm signal pulses until on average 1.2 photons per pulse entered the hollow-core capillary. In Fig. 3 (inset) we plot the APD count rate at $\lambda_o = 610$ nm as a function of delay between the write pulse and the input signal pulse.

At the optimum delay we achieve an SNR of 2.3(1):1 when operating at the ambient temperature (T=295 K). To confirm the absence of FWM noise, in Fig. 3 we plot the count rate of
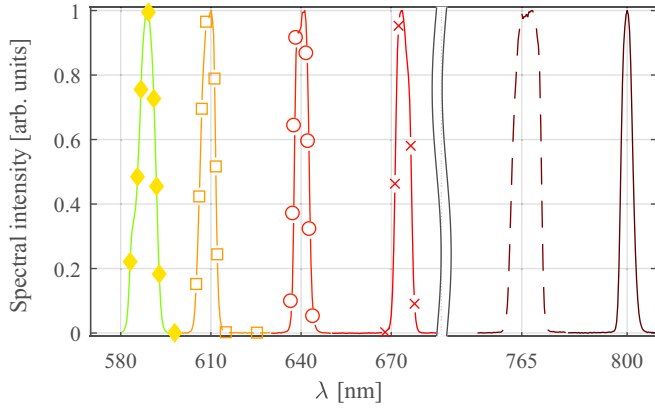
FIG. 2. Plot showing spectra of the write pulse at $\lambda_w = 800\,\text{nm}$ (solid line), input signal at $\lambda_i = 765\,\text{nm}$ (dashed line), and output signals at 673 nm (solid line with cross indicators), 640 nm (solid line with empty circle indicators), 610 nm (solid line with square indicators), and 590 nm (solid line with filled diamond indicators).

the signal and noise as a function of the input read pulse energy. The linear dependence on the read pulse energy confirms that FWM, which varies quadratically with the read pulse energy [27], is not a significant source of noise in the system; instead, the dominant source of noise is spontaneous scattering from thermal population in the $J = 3$ rotational level [27].

Dispersion management is key when optimizing the efficiency and signal-to-noise ratio (SNR) of the frequency conversion process. In order to gain a clearer understanding of the dispersion dependence in hydrogen, we measure the normalized total efficiency as a function of pressure p, or number density N. The Raman coupling strength κ for the write (read) process is proportional to number density N and write (read) pulse energy $\mathcal{E}_w$ ($\mathcal{E}_r$) i.e., $\kappa \propto N\mathcal{E}_w$ [33,40]. We therefore reduce the write and read pulse energies proportionally as we increase the gas pressure in order to keep the Raman coupling strength constant. As can be seen in
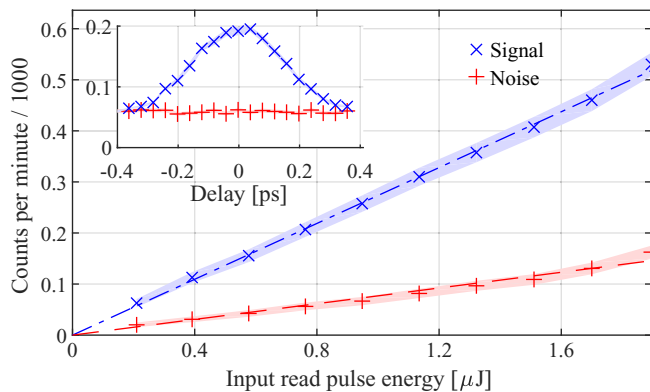

FIG. 3. Plot of the APD counts per minute at $\lambda_o = 610\,\text{nm}$ as a function of input read pulse energy (main figure) and write-signal delay (inset), with the input 765-nm signal on (blue × symbols) and off (red + symbols); standard errors are shown as shaded regions. Linear fits to the signal (blue, dash-dotted line) and noise data (red, dashed line) are also shown.
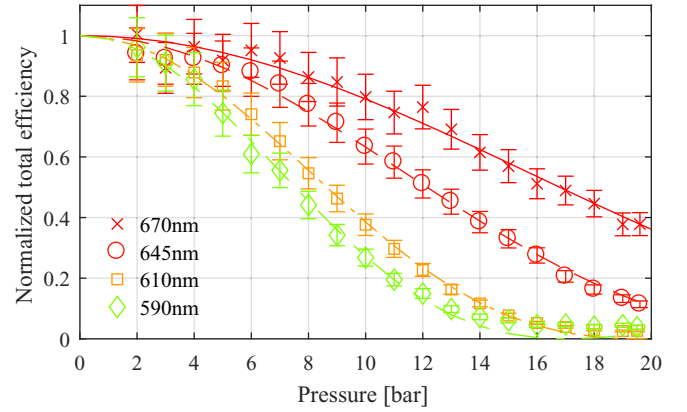

FIG. 4. Plot of the normalized total memory efficiency as a function of pressure p, or phase mismatch $\Delta\mathbf{k}$ since $\Delta\mathbf{k} \propto p$, for several different wavelengths λ_o; standard errors are shown by error bars. The coupling constants were kept fixed by adjusting the input write and read pulse energies according to the gas pressure. Curves show fits of $\text{sinc}^2(|\Delta\mathbf{k}|L/2)$ to the data.

Fig. 4, the normalized conversion efficiency is highest at low pressures before decreasing at higher pressures; furthermore, the normalized efficiency decreases more rapidly when the output signal wavelength is shifted further from the input signal wavelength.

The cause of this behavior is as follows: Background dispersion from the hydrogen molecules introduces a phase mismatch between the wave vector of the excitation created by the memory interaction and the wave vector of the output signal pulse propagating in hydrogen [3,25]. The phase mismatch $\Delta\mathbf{k}$ is given by

$$
\begin{aligned}
\Delta\mathbf{k} &= \mathbf{k}_o - \mathbf{k}_r + \mathbf{k}_w - \mathbf{k}_i, \\
&= p[\{\omega_o\alpha(\omega_o) - (\omega_o - \Omega)\alpha(\omega_o - \Omega)\} \\
&\quad - \{\omega_i\alpha(\omega_i) - (\omega_i - \Omega)\alpha(\omega_i - \Omega)\}]\hat{\mathbf{z}}/c, \quad (1)
\end{aligned}
$$

where $\mathbf{k}(\omega) = (\omega n(\omega)/c)\hat{\mathbf{z}}$ is the wave vector at frequency ω, n is the refractive index, $\hat{\mathbf{z}}$ is a unit vector along the capillary axis, and we have used $n(\omega) = 1 + p\alpha(\omega)$ [41]; additional dispersion from the capillary is negligible. Since $\omega_o > \omega_i$ and $\alpha(\omega)$ is a smoothly increasing function from the infrared to the ultraviolet, $\Delta\mathbf{k}.\hat{\mathbf{z}} > 0$. Increasing the pressure therefore increases the phase mismatch and reduces the normalized efficiency. The expected functional form of this dependence is [25]

$$
\eta_{\text{tot}} = \eta_{\text{tot}}^{\max} \times \text{sinc}^2\left(\frac{|\Delta\mathbf{k}|L}{2}\right), \quad (2)
$$

where $\eta_{\text{tot}}^{\max}$ is the maximum normalized efficiency for a given frequency shift. Using the known dispersion parameters for hydrogen [41], and with the propagation distance L set as a free parameter, we fit Eq. (2) to each data set and obtain good agreement (see Fig. 4).

While the normalized conversion efficiency peaks at zero pressure where the dispersion is lowest, the optimal total conversion efficiency for a given wavelength shift will be at a higher pressure since the coupling strength of the write and read processes each increase linearly with density. Finding

TABLE I. Conversion efficiencies η_{tot} to λ_o and SNR for mean input photon number per pulse $\langle n_{in} \rangle$ at $\lambda_i = 765$ nm, with nominal gas temperature T_{nom} and pressure p.

λ_o (nm)	p (bar)	η_{tot}	$\langle n_{in} \rangle$	SNR	T_{nom} (K)
673	10	0.10(3)	1.1(1)	1.8(2):1	295
640	6	0.07(2)	1.3(1)	2.1(2):1	295
610	3	0.07(2)	1.2(1)	2.3(3):1	295
590	1	> 0.004	1.3(1)	2.1(2):1	295
640	6	–	1.0(1)	4.0(1):1	195

the optimal conversion efficiency therefore involves balancing the competing factors of the coupling strength and the phase mismatch each increasing with density. Optimizing the SNR at the single-photon level is more straightforward, however. Spontaneous Raman scattering from thermal population in the $J = 3$ level is the dominant source of noise; this process is not limited by phase matching constraints. Furthermore, the coupling strength for spontaneous scattering increases linearly with density, as with that of the read process [40]. As a result, when working at the single-photon level, for a given frequency shift we must select a gas pressure such that $\mathrm{sinc}^2 (|\Delta \mathbf{k}| L/2) \approx 1$ to achieve the highest possible SNR; we use the data from Fig. 4 to select a suitable pressure for each measurement.

Table I shows a summary of our results. Operating in ambient conditions at $T = 295 \, K$, we achieve a SNR of approximately 2:1 for mean input photon numbers of $\langle n_{in} \rangle = 1.1$–1.3. In order to achieve this SNR, the operating pressure was reduced for larger frequency shifts. As a result, the conversion efficiency reduced from $\eta_{tot} = 0.10(3)$ when shifting to 673 nm to < 0.01 when shifting to 590 nm. We reduced the temperature to a nominal value of $T = 195 \, K$ by placing the central 20 cm of the gas cell in a dry ice bath. After cooling, we measured an SNR of 4.0(1):1 for a mean input photon number of $\langle n_{in} \rangle = 1.0(1)$ when shifting to $\lambda_o = 640$ nm. The average *conditional* fidelity for conversion of a qubit is expected to be $F_{avg} = 1 - 1/\mathrm{SNR}$, yielding $F_{avg} = 0.75$ for the cooled sample, which exceeds the threshold of

2/3 for a purely classical device [7,42,43]. The SNR could be significantly improved by further cooling. For example, using Boltzmann statistics, we estimate that cooling the whole gas sample to $T = 77 \, K$ in a liquid nitrogen bath would reduce the noise by a factor of ≈ 3300 from the ambient conditions, giving noiseless frequency conversion. In the present setup, the efficiency is limited by imperfect mode matching of the memory interaction [44] and the $\approx 50\%$ transmission loss of the capillary; transmission loss could be significantly reduced by using structured hollow-core fibers [45,46], while pulse shaping techniques [47] could be used to further improve the mode matching.

In conclusion, we have demonstrated frequency conversion at the quantum level using a Raman quantum memory based on the rotational levels of hydrogen molecules. We shifted THz-bandwidth, fs-duration photons at 765 nm continuously over wavelengths spanning from 673 to 590 nm—a range of 62 THz, and an absolute shift of up to 116 THz. Given read pulses of appropriate wavelengths, smaller shifts are also possible; the memory thus supports absolute shifts over a tuning range $\approx \pm 100$ THz from the input signal wavelength, which may be tuned throughout the visible and infrared. The dominant source of noise is spontaneous scattering from thermally excited phonons. By cooling the gas sample to a nominal temperature of $T = 195 \, K$ we were able to achieve a signal-to-noise ratio of 4.0(1):1. Cooling the gas to liquid nitrogen temperatures would render thermal noise negligible, raising the prospect of noiseless frequency conversion across a broad spectral range. Hydrogen's low dispersion extends from infrared right through to ultraviolet wavelengths, making this a powerful platform for frequency conversion. In particular, it should be possible to frequency shift from telecom wavelengths to near-infrared regions of the spectrum where many nascent quantum technologies operate.

[1] P. A. Franken, A. E. Hill, C. W. Peters, and G. Weinreich, Phys. Rev. Lett. **7**, 118 (1961).

[2] N. Bloembergen, Selected Topics IEEE J. Quantum Electron. **6**, 876 (2000).

[3] N. Bloembergen, Am. J. Phys. **35**, 989 (1967).

[4] M. D. Eisaman, J. Fan, A. Migdall, and S. V. Polyakov, Rev. Sci. Instrum. **82**, 071101 (2011).

[5] F. Bussières, N. Sangouard, M. Afzelius, H. de Riedmatten, C. Simon, and W. Tittel, J. Mod. Opt. **60**, 1519 (2013).

[6] K. Heshami, D. G. England, P. C. Humphreys, P. J. Bustard, V. M. Acosta, J. Nunn, and B. J. Sussman, J. Mod. Opt. **63**, 2005 (2016).

[7] L.-M. Duan, M. D. Lukin, J. I. Cirac, and P. Zoller, Nature (London) **414**, 413 (2001).

[8] N. Sangouard, C. Simon, H. de Riedmatten, and N. Gisin, Rev. Mod. Phys. **83**, 33 (2011).

[9] E. Knill, R. Laflamme, and G. J. Milburn, Nature (London) **409**, 46 (2001).

[10] J. Lavoie, J. M. Donohue, L. G. Wright, A. Fedrizzi, and K. J. Resch, Nat. Photonics **7**, 363 (2013).

[11] M. T. Rakher, L. Ma, O. Slattery, X. Tang, and K. Srinivasan, Nat. Photonics **4**, 786 (2010).

[12] M. T. Rakher, L. Ma, M. Davanco, O. Slattery, X. Tang, and K. Srinivasan, Phys. Rev. Lett. **107**, 083602 (2011).

[13] S. Tanzilli, W. Tittel, M. Halder, O. Alibart, P. Baldi, N. Gisin, and H. Zbinden, Nature (London) **437**, 116 (2005).

[14] T. Guerreiro, A. Martin, B. Sanguinetti, J. S. Pelc, C. Langrock, M. M. Fejer, N. Gisin, H. Zbinden, N. Sangouard, and R. T. Thew, Phys. Rev. Lett. **113**, 173601 (2014).

[15] K. De Greve, L. Yu, P. L. McMahon, J. S. Pelc, C. M. Natarajan, N. Y. Kim, E. Abe, S. Maier, C. Schneider, M. Kamp *et al.*, Nature (London) **491**, 421 (2012).

[16] R. Ikuta, Y. Kusaka, T. Kitano, H. Kato, T. Yamamoto, M. Koashi, and N. Imoto, Nat. Commun. **2**, 1544 (2011).

[17] B. Kambs, J. Kettler, M. Bock, J. N. Becker, C. Arend, A. Lenhard, S. L. Portalupi, M. Jetter, P. Michler, and C. Becher, Opt. Express **24**, 22250 (2016).

[18] X. Fernandez-Gonzalvo, G. Corrielli, B. Albrecht, M. Grimau, M. Cristiani, and H. de Riedmatten, Opt. Express **21**, 19473 (2013).

[19] H. J. McGuinness, M. G. Raymer, C. J. McKinstrie, and S. Radic, Phys. Rev. Lett. **105**, 093604 (2010).

[20] A. S. Clark, S. Shahnia, M. J. Collins, C. Xiong, and B. J. Eggleton, Opt. Lett. **38**, 947 (2013).

[21] B. A. Bell, J. He, C. Xiong, and B. J. Eggleton, Opt. Express **24**, 5235 (2016).

[22] Q. Li, M. Davanço, and K. Srinivasan, Nat. Photonics **10**, 406 (2016).

[23] J. T. Hill, A. H. Safavi-Naeini, J. Chan, and O. Painter, Nat. Commun. **3**, 1196 (2012).

[24] A. Radnaev, Y. Dudin, R. Zhao, H. Jen, S. Jenkins, A. Kuzmich, and T. Kennedy, Nat. Phys. **6**, 894 (2010).

[25] K. A. Fisher, D. G. England, J.-P. W. MacLean, P. J. Bustard, K. J. Resch, and B. J. Sussman, Nat. Commun. **7**, 11200 (2016).

[26] D. G. England, P. J. Bustard, J. Nunn, R. Lausten, and B. J. Sussman, Phys. Rev. Lett. **111**, 243601 (2013).

[27] P. J. Bustard, D. G. England, K. Heshami, C. Kupchak, and B. J. Sussman, Opt. Lett. **41**, 5055 (2016).

[28] A. V. Sokolov and S. E. Harris, J. Opt. B: Quantum Semiclass. Opt. **5**, R1 (2003).

[29] N. Zhavoronkov and G. Korn, Phys. Rev. Lett. **88**, 203901 (2002).

[30] C. Wang, C. Kurtsiefer, H. Weinfurter, and B. Burchard, J. Phys. B **39**, 37 (2006).

[31] F. Jelezko, C. Tietz, A. Gruber, I. Popa, A. Nizovtsev, S. Kilin, and J. Wrachtrup, Single Mol. **2**, 255 (2001).

[32] W. Tittel, M. Afzelius, T. Chaneliére, R. Cone, S. Kröll, S. Moiseev, and M. Sellars, Laser & Photonics Reviews **4**, 244 (2010).

[33] A. E. Kozhekin, K. Mølmer, and E. Polzik, Phys. Rev. A **62**, 033809 (2000).

[34] K. F. Reim, J. Nunn, V. O. Lorenz, B. J. Sussman, K. C. Lee, N. K. Langford, D. Jaksch, and I. A. Walmsley, Nat. Photon. **4**, 218 (2010).

[35] G. Herzberg, *Spectra of Diatomic Molecules, Molecular Spectra and Molecular Structure* (Van Nostrand, Princeton, 1950), Vol. 1.

[36] D. A. Long, *The Raman Effect: A Unified Treatment of the Theory of Raman Scattering by Molecules* (John Wiley & Sons, New York, 2002), pp. 153–219.

[37] R. W. Minck, E. E. Hagenlocker, and W. G. Rado, Phys. Rev. Lett. **17**, 229 (1966).

[38] M. Bradler, P. Baum, and E. Riedle, Appl. Phys. B **97**, 561 (2009).

[39] E. Marcatili and R. Schmeltzer, Bell Syst. Tech. J. **43**, 1783 (1964).

[40] M. G. Raymer and J. Mostowski, Phys. Rev. A **24**, 1980 (1981).

[41] M. Karplus, J. Chem. Phys. **41**, 880 (1964).

[42] S. Massar and S. Popescu, Phys. Rev. Lett. **74**, 1259 (1995).

[43] C. Simon, M. Afzelius, J. Appel, A. Boyer de la Giroday, S. J. Dewhurst, N. Gisin, C. Y. Hu, F. Jelezko, S. Kröll, J. H. Müller, J. Nunn, E. S. Polzik, J. G. Rarity, H. De Riedmatten, W. Rosenfeld, A. J. Shields, N. Sköld, R. M. Stevenson, R. Thew, I. A. Walmsley, M. C. Weber, H. Weinfurter, J. Wrachtrup, and R. J. Young, Eur. Phys. J. D **58**, 1 (2010).

[44] J. Nunn, I. A. Walmsley, M. G. Raymer, K. Surmacz, F. C. Waldermann, Z. Wang, and D. Jaksch, Phys. Rev. A **75**, 011401 (2007).

[45] F. Couny, F. Benabid, P. J. Roberts, P. S. Light, and M. G. Raymer, Science **318**, 1118 (2007).

[46] P. S. J. Russell, P. Hölzer, W. Chang, A. Abdolvand, and J. Travers, Nat. Photonics **8**, 278 (2014).

[47] A. Monmayrant, S. Weber, and B. Chatel, J. Phys. B: At., Mol. Opt. Phys. **43**, 103001 (2010).